NIH Public Access
Author Manuscript
Neuron. Author manuscript; available in PMC 2009 September 25.

Published in final edited form as:
Neuron. 2008 September 25; 59(6): 1009–1023. doi:10.1016/j.neuron.2008.07.040.

Testing Odor Response Stereotypy in the *Drosophila* Mushroom Body

Mala Murthy, **Ila Fiete**, and **Gilles Laurent**
Division of Biology, California Institute of Technology, Pasadena, California, 91125

SUMMARY

The mushroom body is required for olfactory learning in flies. Its principal neurons, the Kenyon cells (KCs), form a large cell population, usually divided into three classes(α/β, α'/β', and γ) based on anatomical criteria. Both neuronal populations from which their olfactory input derives, the projection neurons (PNs) and the presynaptic partners of the PNs, the olfactory sensory neurons, can be identified individually by their glomerular projections, the expression of specific genes, and their odor responses. We ask here whether KCs are similarly identifiable individually. We focused on a subset of ~23 genetically labeled α/β KCs, and recorded their responses to odors using whole-cell patch-clamp *in vivo*. Response profiles across this sample provided no evidence for repeats across animals. Further, across-animal responses were as diverse within the genetically-labeled subset as across all KCs in a larger sample. By contrast, recorded PN odor responses clustered by glomerular type. Using these PN responses as inputs to a simple KC model, we find that measured inter-fly PN response variability combined with stereotyped PN-to-KC connectivity cannot explain the absence of KC odor response stereotypy. These results suggest differences in PN-to-KC connectivity across individual flies.

Keywords

Drosophila; olfaction; mushroom body; electrophysiology; stereotypy

INTRODUCTION

Recent studies in mice and flies have revealed astonishing order in the spatial organization of the early olfactory system. Olfactory sensory neurons (OSNs) that express the same olfactory receptor genes converge to the same glomerulus in the antennal lobe (flies) or olfactory bulb (mice). The glomeruli are in turn distributed in consistent spatial patterns, in which neighborhood relationships are conserved across individuals (Couto et al., 2005; Dobritsa et al., 2003; Fishilevich and Vosshall, 2005; Laissue et al., 1999; Mombaerts et al., 1996; Ressler et al., 1994; Vassar et al., 1994). In flies, the second-order neurons (PNs) can be classified anatomically by the glomerulus they innervate and consequently, by the OSN type to which they are postsynaptic (Jefferis et al., 2001; Jefferis et al., 2004). Not only is this anatomical/molecular mapping reproducible across individuals, but it correlates well with functional stereotypy. Imaging and electrophysiological studies in both the antennal lobe and olfactory bulb have shown reproducible odor responses across animals (Belluscio and Katz, 2001; de

Corresponding Author: Gilles Laurent (laurentg@caltech.edu; 626-395-2798).

Publisher's Disclaimer: This is a PDF file of an unedited manuscript that has been accepted for publication. As a service to our customers we are providing this early version of the manuscript. The manuscript will undergo copyediting, typesetting, and review of the resulting proof before it is published in its final citable form. Please note that during the production process errors may be discovered which could affect the content, and all legal disclaimers that apply to the journal pertain.

NIH-PA Author Manuscript
NIH-PA Author Manuscript
NIH-PA Author Manuscript

NIH-PA Author Manuscript

NIH-PA Author Manuscript

NIH-PA Author Manuscript

Bruyne et al., 2001; Hallem et al., 2004; Meister and Bonhoeffer, 2001; Ng et al., 2002; Rubin and Katz, 1999; Uchida et al., 2000; Wang et al., 2003; Wilson et al., 2004). Such functional stereotypy in *Drosophila* PNs is surprising given that—due, in part at least, to interactions between glomerular channels—these neurons are tuned more broadly than their presynaptic partners (Olsen et al., 2007; Shang et al., 2007; Wilson et al., 2004). It suggests significant stereotypy in the synaptic connections between OSNs, PNs, and local neurons within the antennal lobe.

We ask here whether precise anatomical and functional specification of antennal lobe circuits continues in the next relay, the mushroom body. This issue is generally important because it relates to the specification of sensory network connectivity: at what level (if at all) does the order that exists in early circuits break down, such that connections and cellular properties become specific to each individual animal? In insects, PNs form excitatory synapses with a large population of neurons in the mushroom body (MB), a structure involved in learning and memory (Davis, 2005; Gerber et al., 2004; Margulies et al., 2005). We examine whether these targets, called Kenyon cells (KCs), are individually stereotyped across animals. What is the evidence thus far? In *Drosophila*, initial morphological studies found little stereotypy in the PN projections to the MB, especially when compared with the PNs' other axonal projections in the lateral horn (Marin et al., 2002; Wong et al., 2002). More recent results suggest some broad "zonal" stereotypy, both for PN axons and for KC dendritic fields in the MB calyx (Jefferis et al., 2007; Lin et al., 2007; Tanaka et al., 2004; Zhu et al., 2003). In these studies, PNs were identified by the glomerulus from which they originate, while KCs are broadly categorized into one of three classes, based on their axonal projections. Recent calcium imaging studies on KCs in flies also suggest broad stereotypy (Wang et al., 2004). Thus, while available data indicate some regional anatomical stereotypy of projections within MBs, they remain inconclusive about the degree of variability of inputs to individual KCs across flies. Further, even if the wiring diagram between PNs and KCs was known in great anatomical detail and shown to be stereotyped across flies, we still could not conclude that KC odor responses must be stereotyped. To determine whether individual KCs can be identified across animals in the same way that PNs can, functional recordings are required.

We tackled this issue of KC identifiability using functional assays and *Drosophila* mushroom body neurons for three main reasons. The first is that MBs, while small when compared with areas of mammalian cerebral cortex, comprise a large population of similar neurons (~2,500 KCs per hemisphere). KCs can be grouped into three distinct morphological classes (α/β, α'/β', and γ) based on adult axonal projection patterns and birth order (Crittenden et al., 1998; Lee et al., 1999), but they are too similar morphologically to one another within these classes to provide clues as to the existence of identifiable individuals. Yet, the functional stereotypy of PNs indicates that, if the detailed connectivity between PNs and KCs is identical across flies, KCs could be functionally stereotyped as well. Failing to find functional stereotypy in KCs could thus suggest variable input patterns across flies. The second reason is that MBs are required for learning in flies and honeybees (Davis, 1993; Heisenberg et al., 1985; Menzel, 1983; Quinn et al., 1974): molecules implicated in learning are concentrated there (Han et al., 1992; Nighorn et al., 1991), experience can induce substantial structural changes to the MB (Heisenberg et al., 1995; Technau, 1984), and interfering with the function of the MB prevents memory formation or retrieval (Dubnau et al., 2001; McGuire et al., 2003; Zars et al., 2000). Because synapses within the MB are thought to be plastic, odor representations by KCs, by their targets or both might differ across individuals, precluding identification based on tuning. The third reason is that *Drosophila* offers the unique opportunity to examine functional stereotypy within a large network of like neurons, by exploiting the use of genetically encoded markers, isogenic backgrounds and homogenous rearing conditions, and *in vivo* electrophysiology.

NIH-PA Author Manuscript

NIH-PA Author Manuscript

NIH-PA Author Manuscript

Here, we have tested whether individual KCs, characterized by their response profiles, can be recognized from one fly to the next, and conclude that the precise circuit specification seen in the antennal lobe is likely absent at the next stage of processing.

RESULTS

A GAL4 line with restricted expression enables *in vivo* recordings from potential Kenyon cell replicates across flies

We define "functionally replicated" or "individually identifiable" KCs as neurons from different individuals that belong to the same morphological class, have similar lineages, are marked by the same genetic marker, and have similar physiological tuning profiles. To record from potential KC functional replicates across flies, we used a GAL4 line with restricted expression in a small subset of KCs. The *Drosophila* GAL4/UAS system (Brand and Perrimon, 1993) allows for spatial control over transgene expression, based on the promoter regulating the GAL4 insert. GAL4 line NP7175 (Tanaka et al., 2004) is an insertion in the 5' UTR of the CG3095 gene (also known as *halfway* or *singed wings* (Schwartz et al., 2004)); when crossed to a GFP reporter construct, a small number of KCs that project to the centers of the α/β lobes are labeled (Figure 1A). Kenyon cells and glial cells of the MB are sequentially derived from four neuroblasts, and each neuroblast is sufficient to generate autonomously all of the axonal substructures (α/β, α'/β', and γ) of the MB (Ito et al., 1997; Lee et al., 1999). KCs born early are pushed, through multiple rounds of cell division, to the outermost regions of the concentric soma layer (Kurusu et al., 2002). Fortuitously, NP7175 marks KCs that are born late in mushroom body development; thus, they remain clustered close to their neuroblast of origin, enabling the reliable distinction of four clusters or clonal units. Each clonal unit occupies a distinct dendritic territory within the MB calyx, defined by the axes of the brain (Zhu et al., 2003). In particular, late-born α/β neurons neither cross these clonal boundaries within the calyx nor project to a fourfold region of the calyx that contains dendrites of KCs from all clonal units. Based on these characteristics of mushroom body development, the KCs labeled by NP7175 can be consistently divided into four clonal units of few neurons (Figure 1B).

We focused on the left hemisphere (when viewed from the posterior surface) and lateral posterior clonal unit (L-LP). KCs of the posterior clonal units are easier to reach with electrodes because they lie closer to the brain surface. We performed *in vivo* whole-cell patch-clamp recordings of KCs in intact one-day-old female flies, raised at constant temperature and relative humidity (see methods). We chose one-day-old flies to limit adult olfactory experience and thus, hopefully limit inter-fly variability. Flies of this age perform robustly in olfactory learning and memory assays (Tamura et al., 2003), indicating that the mushroom body is functional.

We filled each recorded KC with biocytin (Figure 1C) to verify after the experiment that it was an NP7175 (GFP^+) KC of the L-LP subset—fills of 18 GFP^- KCs (with somata adjacent to GFP^+ KCs) contained projections not to the centers of the α/β lobes, but to separate regions of mostly the α/β and occasionally the α'/β' and γ lobes. GFP^+ KCs, in contrast to these GFP^- cells, were distinct in their axonal morphology—all GFP^+ KCs possessed no side branch in the alpha lobe and at most one (in 6/27 fills) side branch at the tip of the beta lobe (data not shown). Further indicating that NP7175-driven expression is consistent from fly to fly, GFP expression co-localized (in 14 brains) with a label for F-actin (Phalloidin), enriched in a small number of KC fibers in the centers of the α/β lobes (Figure 1D). Previous observations of KCs labeled by NP7175 counted approximately 60 cells per hemisphere (~15 labeled KCs per clonal unit) (Tanaka et al., 2004). We repeated these observations for our experimental conditions and genotype (see methods), and counted either the number of cells in only the L-LP clonal unit, or in any of the 8 clonal units from both hemispheres (Figure 1E). With both methods, we found 23 ± 0.73 (mean ± SEM) labeled cells per clonal unit, with small variability around

NIH-PA Author Manuscript

NIH-PA Author Manuscript

NIH-PA Author Manuscript

this number (SD=3.27, min=20, max=31). These data collectively argue against the possibility that NP7175 labels different subsets of α/β KCs in each fly.

If KCs are individually identifiable neurons, how many recordings are needed to ensure repeated samplings of the "same" KCs across flies? With roughly 23 GFP^+ KCs per clonal unit and recordings from one GFP^+ L-LP neuron each in 27 flies, there must be a minimum of 13 replicates (non-singletons, such as doublets, triplets, etc.), with P>0.99, and an average of 18.5 replicates in the data set (Figure 1F). Even if there are as many as 31 GFP^+ KCs per clonal unit, the maximum number counted in one fly, there should be at least 9 non-singletons in our data set (Figure 1G). Our recordings were likely biased towards KCs with posterior somata and against KCs with low GFP expression. If the distributions of these somata or GFP levels within each clonal unit are not random, we may have sampled from a smaller subset of the 23 labeled cells, resulting in even higher probabilities of non-singletons. With this expectation, we recorded from KCs in 50 flies and looked for functional repeats among 27 GFP^+ L-LP recordings.

Odor response profiles vary across the GFP^+ L-LP KC recordings

Using whole-cell patch-clamp, we measured KC responses (below and above firing threshold) to a diverse odor set. Because we held KCs at approximately −60mV, we first assessed the relationship between holding potential and voltage changes during odor responses. This test was to ensure that no major non-linearity occurs around this holding potential, which could affect our inter-cell comparisons (based on intrinsic firing frequency and membrane voltage). Figure 2A plots this relationship for two KCs and finds good linear fits over the range between −40 and −100mV. This indicates that KC synaptic responses in this range are mainly affected by driving force, and not by voltage-dependent rectifying or amplifying non-linearities.

We challenged KCs with a set of 12 odors at 3 concentrations (10- 100- and 1000- fold dilutions). Odors were presented as 1s pulses during 20s trials in blocks of 6 trials each, on average. We characterized the odor response profiles of 50 KCs (KC1-KC27: GFP^+ L-LP, KC28-KC32: GFP^+ other clonal units, and KC33-KC50: GFP^-) by examining both spiking and subthreshold odor responses (Figure 2B). In all analyses, we omitted the first trial because it can differ significantly from subsequent ones (Stopfer and Laurent, 1999). Odor-evoked spiking responses are typically sparse; KCs respond with few spikes to only a few (if any) of the odors presented (Figure 2C; (Perez-Orive et al., 2002; Turner et al., 2007). "Subthreshold" responses (red, Figure 2B), in contrast, were low-passed voltage responses (see methods) and thus include both sub- and supra- threshold odor responses and trials; they are the most complete description of each cell's tuning. They also decrease the probability of wrongly classifying two KCs as different if the only difference between them was their firing threshold, holding potential, or input resistance. A few examples are shown in Figure 2D, illustrating the onsets, amplitudes and shapes of some of the profiles observed across the 27 GFP^+ L-LP KCs. With a few KCs, we presented the same odor at the beginning (red, Figure 2E) and end (black, Figure 2E) of the experiment, to control for response stability.

Spiking Responses—For analysis of spiking responses, a KC was considered responsive to an odor if it produced at least one action potential in the period 0–2s following stimulus onset, on at least 3 trials. If a KC was tested with *n* odors, its response profile could be described as a binary *n*-bit vector (1 for response (red), 0 for no response (gray); Figure 3A). As in the locust (Stopfer et al., 2003), KCs in *Drosophila* can be odor selective and concentration insensitive (e.g., KC11, odor 5; Figure 3A), or odor and concentration selective (e.g., KC1, odor 8; Figure 3A). KCs could then be compared by measuring the Euclidean distances between their spiking response profiles (Figure 3B). Euclidean distances were calculated with only the odors tested in common in each KC pair, and a distance of 0 (black; Figure 3B) indicates

NIH-PA Author Manuscript

NIH-PA Author Manuscript

NIH-PA Author Manuscript

identical odor response profiles. Only 1 pair among the 27 recorded GFP^+ L-LP KCs had the same (and non-zero) profiles: KC6 and KC21 (9 common odors). The more stringent we made the criteria for a spiking response, the fewer identical profiles we found (data not shown). The probability of response (percentage of odors eliciting a response) was 18.6% for the GFP^+ L-LP KCs, compared to 49% for the GFP^- KCs. Thus, while only one pair among the GFP^+ L-LP KCs possessed identical spiking responses, the GFP^+ L-LP KCs were similar to one another as a group, in that they responded to fewer odors overall. However, using response criteria from a previous study on locust KCs (Perez-Orive et al.), the probability of response for the GFP^+ L-LP KCs dropped to 6.7%, matching the response probability (also using these criteria) for *Drosophila* α/β KCs tested with a different odor set (Turner et al., 2007). Thus, even though our assignment of positive KC responses was loose, only one repeat was found among all 351 possible pairs from 27 GFP^+ L-LP KCs.

Subthreshold Responses—Because so many (20/50) of the KCs in our data set showed no spiking response to any odors tested (Figure 3A), we could not determine the number of functional replicates among the GFP^+ L-LP KCs using spiking responses alone. We therefore examined subthreshold KC response profiles, a measure more directly reflective of the input KCs receive from PNs. Subthreshold responses of a KC to an odor were measured as an average across trials of the filtered (to remove spikes) and baseline-subtracted membrane voltage (red, Figure 2B). We characterized each KC's response profile as a concatenated vector of *n* voltage traces (one trace for each of *n* odors; see supplemental data for examples). Pairwise comparisons were made by measuring the correlation distance (one minus the mean-subtracted cross-correlation between the tuning vectors; see methods) for all odors tested in common between each pair of neurons. Thus, two response profiles that differed only in their amplitudes would be classified as identical (distance(corr)=0). The minimum and mean number of odors tested in common were 3 and 10 over all pairs, respectively (see supplemental data for justification of minimum). The pairwise analysis was carried out over all 50 KCs in our data set, and results are shown in the matrix in Figure 3C.

As with spiking profiles, subthreshold responses were as (or more) different across the GFP^+ L-LP KCs as they were between them and GFP^- KCs (Figure 3D). To ensure that such differences were not due to excessive trial-trial variability, we also measured distances between trials for each KC/odor combination (2,356 trials and 85,328 pairwise comparisons), and found them to be significantly smaller than the inter-KC distances ($p<10^{-87}$; Figure 3D). This indicates that the response of one KC to an odor is closer, on average, to individual trials with that odor than it is to the mean response of another sampled KC to that odor.

Using these pairwise correlation distances, we then performed hierarchical clustering (see methods) to assess similarities between KCs across the entire dataset. The closest linkage distances between KCs were often not between KCs in the GFP^+ L-LP subset (Figure 3E). Notably, KC6 and KC21 had identical spiking odor response profiles (Figure 3B), but did not cluster together based on their subthreshold odor response profiles. Finally, for each KC/odor combination, we split its trials in half, and repeated the above analysis (supplemental data). GFP^+ L-LP KCs grouped well across trials, with a goodness-of-clustering score (see methods), of 96%. This showed again that the inter-trial variability for each KC was much smaller than the differences in responses across different KCs.

In summary, KCs randomly sampled from the GFP^+ L-LP clonal unit in 27 different flies yielded many different physiological profiles for this odor set, and failed to reveal obvious functional repeats. Nevertheless, if input PN responses are variable across flies, KCs may appear to be physiologically dissimilar even if the underlying PN-to-KC wiring is identical across files. To determine how much response variability we should expect across "individually identified" KCs, we thus recorded from the PNs, under the same stimulus conditions.

NIH-PA Author Manuscript

NIH-PA Author Manuscript

NIH-PA Author Manuscript

Measurement of PN odor response variability across flies

PNs are the only known excitatory drive to the KCs (Gu and O'Dowd, 2006; Yasuyama et al., 2002). We characterized PN odor responses in a first step towards testing a simple hypothesis: if connectivity between PNs and KCs is invariant across flies, then the observed functional variability of KCs should be explained by PN odor response variability. We know already that PNs are both morphologically and physiologically identifiable across flies (Wang et al., 2003; Wilson et al., 2004). Here, we quantify response variability across PNs of the same glomerular type, and assess whether this variability is large enough to preclude KC response stereotypy.

We recorded the odor responses of nine PNs innervating the DL1 glomerulus and eight PNs innervating six other glomeruli. These recordings were made in *NP3529-GAL4* flies expressing GFP in, among other cells, 2 DL1 PNs per hemisphere (Tanaka et al., 2004). We challenged flies with the same 12 odors (1/100 dilutions only) tested on KCs and filled each recorded PN with biocytin for post-hoc identification (Figure 4A). One of the recorded DL1 PNs was tested with less than 3 odors shared with some other PNs, and was thus excluded from this part of the analysis. However, all nine DL1 PNs were used in the subsequent KC simulation model (Figure 5).

As with the KCs (Figure 3), we calculated pairwise correlation distances between all recorded PN responses based on spiking (supplemental data) or subthreshold (Figures 4C–4E) odor responses for all odors tested in common between each pair of cells. Distances between responses of PNs of one glomerular type (ie: DL1, VC3, or DM6) were significantly smaller than across PNs of different types (Figure 4D). PNs could easily be clustered by type (Figure 4E), with a goodness-of-clustering score, based on whether nearest neighbors were of the same type, of 100%. These results were statistically similar when spiking responses were used to calculate pairwise distances (supplemental data). Thus, despite the presence of some inter-individual variability between odor responses from PNs of a single glomerular type, it is still possible to observe an excellent match between functional and anatomical groupings among the PN population. Further, our ability to cluster PN responses served as a validation of our analysis methods on the KC recordings. We next used these PN data in a model to determine the expected inter-fly variability of KCs with stereotyped connectivity to PNs (Figure 5A).

Model KCs with realistic PN input variability can be clustered by type

If Kenyon cells are identifiable, we anticipated finding at least 13 functional replicates with $P>0.99$ in our recordings (Figure 1). To determine if our recordings are consistent with the presence of such replicates, we generated model KCs, whose responses were defined by experimental PN data (Figure 5A). If in the model, responses from different KCs of one type (generated from measured inter-fly PN variability) are far more similar to one another than responses from KCs of different types (in the model, a KC type is defined by its specific set of PN inputs), then KCs should be clusterable by type across flies. Further, similarity thresholds derived from the model could be applied to the recorded KCs, to identify possible functional replicates.

PN recordings yielded a total of 81 different measured spiking responses (2s PSTHs), from an average of ~11 odors each tested on 7 different glomerular types (one PN type's responses to different odors were as diverse as different PN types' responses to one odor, based on a clustering analysis (data not shown and (Bhandawat et al., 2007)); each of these responses was treated as equal and distinct in constructing model KC responses. To augment the data set, we added fixed temporal shifts to each recorded PN response (see methods), generating a total of 160 model PN (mPN) responses. Each mPN type response profile consisted of a concatenation of four of these responses, to mimic 4 odors tested on each mPN. To simulate inter-individual

NIH-PA Author Manuscript

NIH-PA Author Manuscript

NIH-PA Author Manuscript

(across-fly) variability for each mPN type, we applied the measured variance across multiple PN recordings in different flies (*e.g*, from DL1) to an mPN type response profile to produce different individual responses per mPN type (see methods). PN:KC convergence in *Drosophila* is estimated to be approximately 10:1 (Turner et al., 2007). To produce model KC (mKC) "subthreshold" responses, we linearly summed different mPN response profiles with convergence factors (N_{conv}) ranging from 5 to 20, using different binary PN:KC weight vectors for each mKC type (Figures 5A and 5B).

mKC types generated with larger N_{conv} were more similar to each other than those generated with smaller N_{conv}, as expected from the law of large numbers (averaging effects). The pairwise distance distribution for mKC odor responses best overlapped the real KC distribution at lower N_{conv} (Figure 5C, black and green curves; Figure 5D, black squares). Inter-individual variances also grew as N_{conv} decreased (Figure 5C, red curves). Consequently, the separation between mKC types (Figure 5C, black curves) and mKC individuals of a type (Figure 5C, red curves) remained generally constant across N_{conv} (Figure 5D, black circles), suggesting that the clusterability of mKCs by type should be independent of N_{conv}. In cases where mKCs pool inputs from multiple mPNs of the same type (*e.g.*, N_{conv}=5*2, or 10 inputs from 5 different PN glomerular types), the type diversity is as great as for N_{conv}=5, but the individual distances are smaller, similar to N_{conv}=10, leading to an even larger separation between type and individual distributions (Figure 5D, open circles and squares).

We next performed hierarchical clustering on the pairwise distances between mKC responses. The resulting goodness-of-clustering scores (see methods), was high and independent of N_{conv} (Figures 5D (red circles) and Figure 5E). These results implied that individual recorded KCs should be recognizable from animal to animal by their subthreshold response profiles, if we hypothesize that PN-to-KC wiring is stereotyped and account for KC response variability as due to PN response variability.

Thresholds derived from the model reveal fewer potential KC functional replicates in the experimental dataset than predicted

By performing hierarchical clustering on the recorded KC subthreshold odor responses, we obtained linkage distances between all 27 GFP+ L-LP KCs in the data set (Figure 3E). Ultimately, we wished to determine if any of these linkages were small enough to indicate functional replicates. To do so, we recreated the experimental sampling procedure (27 recordings from the 23-cell GFP^+ L LP clonal unit) by randomly selecting 27 individual mKCs from 23 mKC types (see methods). We derived similarity thresholds from this sampling experiment and directly applied them to the experimental data.

For each run of the sampling experiment, we calculated pairwise distances between mKC responses, performed hierarchical clustering, and extracted the highest threshold value (gray, Figure 6A) below which all mKCs were correctly grouped by type. The cumulative probabilities of finding functional replicates (non-singletons) below the thresholds for N_{conv}=5, 5*2, and 10 are shown in Figure 6C (blue curves). Because the thresholds were selected to exclude any incorrect groupings, they only captured an average of ~85% (for each N_{conv}) of the model data's actual non-singletons (whose distribution is equivalent to the predicted distribution; Figure 6C, green curve).

We applied the model threshold distributions to the experimental KC tree shown in Figure 6B, and counted the number of KCs with linkage distances below each threshold. This produced probability distributions of the recorded KCs containing *n* non-singletons (Figure 6C, red curves). For direct application of model-derived thresholds to the KC data, a convergence of 5*2 (pooling from 10 PNs of 5 types) was deemed most appropriate because it satisfied the intersection of two constraints: (1)the diversity of mKC types generated from 5 mPN types

NIH-PA Author Manuscript

NIH-PA Author Manuscript

NIH-PA Author Manuscript

best matched the recorded KC diversity (Figure 5D) and (2)the net convergence of 10 matched the best estimate of PN:KC convergence (Turner et al., 2007). For N_{conv}=5*2, the probability of identifying ≥6 non-singletons in the model is 1, whereas in the real data, it is <0.01 (Figure 6C). Across convergences, the thresholds identified an average of more than 14 non-singletons among the mKCs, but fewer than 3 among the real data (Figure 6C, inset). Based on our model, it is thus extremely unlikely that the recorded data represent samples from a set of functionally stereotyped KCs. These findings are consistent with the observation that the closest distances between recorded odor responses in our full data set are between GFP^+ L-LP and GFP^- KCs, rather than between GFP^+ L-LP KCs (Figure 3).

Because our analyses indicated that measured PN response variability combined with stereotyped PN:KC connectivity across individuals cannot account for the variability of KC responses observed in the experimental data, we explored how much variation in PN:KC connections across individuals, in addition to the measured PN response variability, would be required to reproduce the experimental results (Figure 6D). We did this in two ways for N_{conv}=5 (this convergence value found the largest number of potential replicates in the real data), by (i)varying the analog synaptic weight values in a specified PN:KC connection matrix, or (ii)varying the connections themselves. We found that varying the analog weights in a stereotyped connection matrix was not sufficient to reproduce the small number of replicates flagged in the real KC data. If instead, for an mKC type, at least 2 of the 5 PN-to-KC connections in each individual were different, selected randomly from the pool of mPNs, the number of flagged replicates in the model would nearly match the number flagged in the KC recordings. Thus, given measured PN response variability, the degree of variability in PN-to-KC connections in our linear model would have to be at least 40% on the level of individual KCs, to explain the low number of flagged replicates in the real KC data.

DISCUSSION

The olfactory system of *Drosophila* is becoming one of the best-characterized sensory systems in large metazoans (Bhandawat et al., 2007; Hallem and Carlson, 2004; Komiyama and Luo, 2006; Turner et al., 2007; Vosshall and Stocker, 2006; Wang et al., 2003; Wilson et al., 2004). Molecular, anatomical and physiological analyses indicate that its antennal lobe circuits are so precisely organized that OSNs and PNs can both be identified using any of the above characteristics (alone or in combinations). Using electrophysiological recordings and genetic markers, we assessed whether circuit specification continues with similar precision in the mushroom bodies. If identifiable KCs exist, we could reasonably expect to find at least 13 functional replicates (P>0.99) with 27 recordings from among a subset of ~23 genetically labeled neurons. We observed no obvious functional similarities by analyzing both spiking and subthrehsold odor response profiles, nor were the responses of labeled KCs more similar to one another than to responses of unlabeled KCs. To determine how similar responses from identifiable KCs would be, given variability present at earlier stages of the olfactory pathway (*i.e.*, in PN responses), we measured inter-individual variability across PNs of the same glomerular types, and used these data to simulate KC responses (with assumptions detailed and discussed below) across individuals and for many different KC types. After applying clustering thresholds derived from this model to the experimental data, we infer that KC response variability across flies is not explained by PN response variability. KCs may therefore not be individually identifiable, at least in the combined genetic, anatomical and physiological senses that apply to their presynaptic inputs (PNs and OSNs).

Our study suggests that each fly possesses a complement of KCs whose tuning differs from individual to individual. This result is different from (though not in contradiction to) that of a previous study (Wang et al., 2004) in which KC responses to odors were monitored using GCaMP, a genetically-encoded calcium sensor: the somata of KCs that produced a detectable

NIH-PA Author Manuscript

NIH-PA Author Manuscript

NIH-PA Author Manuscript

GCaMP signal to a particular odor (about 10 KCs per odor and per mushroom body) lay in similar positions in different animals after image warping for alignment. Given the small size (<3μm) and large number of KC somata in each mushroom body, we think that KC identification across animals based on such spatial attributes is unlikely.

Could the NP7175 driver itself be variable, labeling a different subset of α/β KCs in each fly? We observed that NP7175-labeled KCs always project to the centers of the α/β lobes and that 23 ± 0.73 clustered KCs per neuroblast clonal unit are labeled in each fly (Figure 1). However, even if we assume that as many as 40 KCs per clonal unit (or 20% of the α/β KCs (Lee et al., 1999)) could be labeled by NP7175 (and a random 23 chosen for expression in each fly), we would expect to find, with only 27 recordings, a minimum of 6 and an average of 13 replicates. This prediction is still inconsistent with our findings.

While we would have liked to repeat our study with another restricted GAL4 line labeling a distinct but comparably sized subset of KCs, we were unfortunately unable to find such a line. The responses of KCs that project to the centers of the α/β lobes (NP7175), however, do not appear unusual among KCs. Similar to other α/β KCs recorded, NP7175 KC responses were sparse and contained few spikes. Further, response probabilities among NP7175 KCs were similar to those in a larger set of α/β KCs (Turner et al., 2007). Finally, we note that a previous report indicating that NP7175 KCs were the only glutamatergic KCs in the mushroom body (Strausfeld et al., 2003) is not supported by immunostaining with an antibody for the *Drosophila* vesicular glutamate transporter (data not shown and (Daniels et al., 2008)). In short, nothing so far indicates that NP7175 KCs are unrepresentative of the larger KC population. We now outline possible mechanisms that could give rise to a lack of functional stereotypy in the mushroom body, and discuss both the caveats and implications of this finding.

Basic Assumptions of the KC model

The results of our model depend on the following assumptions: 1) inter-individual PN response variability is well estimated in our model, 2) summation of PN inputs by KCs is linear, and 3) PN:KC connectivity is stereotyped across animals. Assumption 3 is the one we aimed to test, but the results depend on assumptions 1 and 2, which we discuss in this section.

Our experimental measurements of PN response variability came mostly from DL1 PNs. If other PN responses are more variable across flies, we may have overestimated how well KC responses should cluster. However, recordings from PN duplicates that innervate VC3 and DM6 revealed comparable response variability (Figure 4). In addition, responses to a set of 18 odors in PNs that innervate seven glomeruli, including DL1 (Bhandawat et al., 2007), reveal similar variability. In fact, PN response noise could be even smaller than we report here, because our measure includes both intrinsic variability and variability introduced by recording methods. Also implicit in our model was that response variations are uncorrelated across PNs within one antennal lobe; such intra-individual correlations would produce less averaging in the construction of individual KC responses, generating greater inter-individual variability and poorer clustering than in our mKCs. In the absence of simultaneous recordings from the same *n*-plets of PNs in many individuals, we cannot rule out this possibility.

Our simulation results also assume that KC subthreshold responses represent a linear summation of their inputs. Due to the absence of obvious voltage-dependent nonlinearities (Figure 2A and (Turner et al., 2007)), linear summation in the explored range seems a reasonable hypothesis for *Drosophila* KC integration. In addition, to affect our conclusions, nonlinear summation would have to enhance inter-individual PN variability while not affecting the diversity of model KC types generated with the same nonlinear summing strategy. Finally, by focusing our analyses mostly on subthreshold responses, we ignored spike-generating

NIH-PA Author Manuscript

NIH-PA Author Manuscript

NIH-PA Author Manuscript

nonlinearities. Thus, our data and analyses point instead to differences in PN:KC connectivity across individuals as the most likely cause for the observed variability of KC response profiles.

Connectivity between PN and KC populations

OSN:PN connectivity in the antennal lobe is fully specified and independent of olfactory experience (Berdnik et al., 2006; Jefferis et al., 2004). Whereas beautiful anatomical data exist on PN axonal and KC dendritic projections (Jefferis et al., 2007; Lin et al., 2007; Tanaka et al., 2004; Zhu et al., 2003), their resolution is not sufficient to indicate whether pairwise PN:KC connectivity might be stereotyped across individuals. We did not know, therefore, whether the observed inter-individual variability of KC responses resulted from (i)variability of synaptic weight values in a stereotyped PN:KC connection matrix, (ii)variability of the entries in the connection matrix, or (iii)some combination of the two.

In the first scheme, identified PNs would always contact the same set of KCs (identified by lineage, morphology, and gene expression) but with variable synaptic weights. While such a scheme is consistent with the role of the MB in learning and memory, the influence of individual life histories during larval development is hard to gauge, given the homogeneous rearing conditions of our flies and, possibly more importantly, that both the PNs and KCs active in larval olfaction are completely pruned during metamorphosis (Marin et al., 2005). Further, our modeling results suggest that KC response variability likely does not result from the variability of synaptic weight values alone in a stereotyped PN:KC connection matrix (Figure 6D).

The second possibility is that precise PN-to-KC connectivity forms independently in each animal, possibly with regional spatial specification, as indicated by the identifiability of PN axonal arbors in the calyx (Jefferis et al., 2007) and by the existence of recognizable spatial domains (also called glomeruli) in the developing larval mushroom body (Masuda-Nakagawa et al., 2005). Because PNs are broadly tuned to odors, such a connectivity scheme could still result in the lack of functional stereotypy we observe, in our inability to cluster GFP^+ L-LP α/β KCs within the entire KC dataset, and yet, in the existence of like-responses within larger spatial domains across flies (Wang et al., 2004). Different patterns of connectivity between flies would be particularly interesting if the connections made by the same PNs in the lateral horn were, by contrast, stereotypical—as has been proposed (Jefferis et al., 2007; Marin et al., 2002; Wong et al., 2002). Differences in PN-to-KC connectivity across flies, if the only source of variability, would have to be large (differences of at least ~40% across flies, Figure 6D). However, other possible contributions to KC response variability could, for example, include differences in release probability across time within each odor response, in short-term plasticity, or in the amount of inhibitory input onto each KC. Without information on such differences, we cannot know the extent of their contribution to the observed lack of response stereotypy in individual KCs.

Implications for Memory Formation and KC Readout

Genetic and behavioral evidence in *Drosophila* indicate that KC output is required for the recall of odor memories (Dubnau et al., 2001; Krashes et al., 2007; McGuire et al., 2001; Schwaerzel et al., 2002). However, the functional stereotypy of individual KC responses is not a prerequisite for memory formation. In a system in which associative memories are stored as patterns of synaptic strengths, the identities of the strengthened synapses could be different across animals (i.e., defined without *a priori* specification, but instead by which KCs respond in each animal to the odor producing the associated memory). By extension, a lack of stereotypy might be advantageous from a developmental perspective. The precise wiring of 25,000 synapses (~2500 KCs with 10:1 connectivity between PNs and KCs) would require a complex and precisely controlled mechanism for axonal and dendritic targeting in the calyx. The KCs' own targets, presumably responsible for associating odor-specific KC patterns and reward

NIH-PA Author Manuscript

NIH-PA Author Manuscript

NIH-PA Author Manuscript

signals, likely require that KC odor representations be stable in each individual, not that they be identical across animals. Indeed, in a system responsible for associative learning, variability in the connection matrix used to generate and learn the representations of significant stimuli may be useful to the species at large.

EXPERIMENTAL PROCEDURES

Fly Stocks and Rearing

Flies were reared on standard cornmeal agar medium (Lewis, 1960), at constant temperature (25C) and constant relative humidity (65%). All recordings were made from 24-hour old females. All KC recordings were made from flies of genotype *yw, NP7175; UAS-eGFP2x/CyO*; all PN recordings were made from flies of genotype *UAS-eGFP2x; NP3529-GAL4*. *UAS-eGFP2x* flies (Halfon et al., 2002) were crossed to the above GAL4 lines to generate these stocks; both stocks were isogenized prior to the start of the project.

Drosophila Preparation for Electrophysiology

Flies were anesthetized in a glass vial on ice, inserted into an appropriately shaped hole in aluminum foil, and mounted using melted beeswax (for more details see (Wilson et al., 2004)). For KC recordings, the proboscis was tucked into the head capsule and waxed there, and a small portion of cuticle removed to reveal the posterior side of the brain. The perineural sheath was softened with 0.5mg/ml collagenase (Sigma) and gently picked away. Some head muscles were removed to prevent movement during the recording; spontaneous leg movements typically persisted. The extracellular saline composition was (in mM): NaCl 103, KCl 3, TES 5, $NaHCO_3$ 26, NaH_2PO_4 1, $CaCl_2$ 1.5, $MgCl_2$ 4, trehalose 10, glucose 10, sucrose 9 (pH=7.25, 275 mOsm). The saline was bubbled with 95% O_2 and 5% CO_2 and continuously perfused over the preparation.

Patch-Clamp Recordings *In Vivo*

Whole-cell patch-clamp recordings were obtained from KC or PN somata under visual control using IR-DIC optics, GFP fluorescence and a 40X water-immersion objective on a Zeiss upright microscope. Patch-clamp electrodes were pulled from capillary glass (OD=1.5, ID=1.1) with resistances of 10–12 MOhm for KCs, and 7–8 MOhm for PNs. They were filled with intracellular solution (in mM): K aspartate 150, HEPES 10, MgATP 4, Na_3GTP 0.5, EGTA 1.1 $CaCl_2$ 0.1, biocytin hydrazide 0.5% (Molecular Probes) (pH = 7.3, 265 mOsM). Hyperpolarizing current steps were used throughout recordings to measure intrinsic membrane properties; only KCs with input resistances >10 GOhm and only PNs with input resistances >500 MOhm were used for analysis. Recordings from PNs with no odor-evoked spiking responses to any tested odors (4/33 recordings) were not included in the analysis, as it was assumed that the antennal nerve (exposed in the dissection required to reach PN somata) had been damaged in these preparations. All cells were held between −55mV and −70mV, in current-clamp mode, using an Axoclamp-2B amplifier, and voltage signals were acquired in IGOR Pro (Wavemetrics, Inc.) at 10kHz via a National Instruments A–D board.

Physical access to PN somata for whole-cell recording sometimes required the removal of a few overlaying somata. Because PNs operate in local circuits, these occasional PN or LN injuries might have affected the recorded PN responses. While smaller, KC somata offered easier access; likely few were removed during each dissection. In addition, KCs do not, as far as we know, interact with each other in the calyx, and thus inter-individual variability of KC responses would not be, by contrast with those of PNs, subject to these technical issues. Experimental sources of variability in PNs, however, would only increase our estimate of inter-individual PN response noise.

NIH-PA Author Manuscript

NIH-PA Author Manuscript

NIH-PA Author Manuscript

Odor Delivery

Odors were prepared and delivered as described previously (Wilson et al., 2004). Odors were presented to the fly's antenna in air (at 1/10, 1/100, and 1/1000 final dilutions in paraffin oil and air) using a custom-designed olfactometer. Odor pulses (typically 6 trials per odor) were 1s long, and spaced 21s apart. The odors used in this study were: (1)ethyl acetate; (2) benzaldehyde; (3)proprionic acid; (4)linalool; (5)ethyl butyrate; (6)1-hexanol; (7)1-octen-3-ol; (8)2-heptanone; (9)isoamyl acetate; (10)2,3 butanedione; (11)methyl salicylate; (12) hexanal; (13)methanol; (14)ethanol. Not shown but also tested in several experiments, including all PN recordings, were 2 control stimuli: paraffin oil alone and an empty vial.

Immunohistochemistry

Adult brains were dissected in 1x PBS and stored on ice until fixing in 3.7% formaldehyde, 100mM KPO_4 (pH 6.8), 450mM KCl, 150mM NaCl, 20mM $MgCl_2$ for 30–40 minutes. Anti-FasII (DSHB) was used at 1:100, Anti-nc82 (DSHB) at 1:10, AlexFluor568-conjugated streptavidin (Molecular Probes) at 1:150, and AlexaFluor568-conjugated Phalloidin (Molecular Probes) at 1:200. Secondary antibodies (Molecular Probes) used were AlexaFluor568 goat anti-mouse and AlexaFluor633 goat anti-mouse.

Cell Counting

Kenyon cells labeled by NP7175-GAL4 were counted in brains that had been dissected and fixed on the same day. Brains were oriented such that the anterior side faced the slide. Images were acquired with identical and non-saturating settings for all brains on a Zeiss LSM 510 upright confocal microscope, and cells were counted by hand using the same acquisition software. These images, at brightness settings > 45 (full range: 0–100), consistently revealed more cells than could be visualized on the electrophysiology rig, using a fluorescence microscope.

Data Analysis

All data analysis was carried out in either IGOR Pro (Wavemetrics, Inc.) or Matlab (The Mathworks, Inc.).

Spiking response—peri-stimulus time histograms (PSTHs) were formed by first detecting spikes by applying a threshold to the first derivative of each whole-cell voltage trace. Detected spikes for each trial were then smoothed with a 30ms Gaussian filter to produce a PSTH for each trial (333Hz final sampling rate). These PSTHs were then trial-averaged, and the odor response period + 1s was used for analysis. For PNs only, a 1s period of baseline was subtracted from each trial before averaging.

Subthreshold odor response—Each voltage trace was smoothed with a 30ms moving-average boxcar filter to remove spikes (spike waveforms at the soma are typically 15–20ms wide, due to low-pass filtering by the unexcitable and high-resistance soma membrane). These smoothed traces were then trial-averaged, and the odor response period + 1s was used for analysis. For both KCs and PNs, a 1s period of baseline was subtracted from each trial before averaging.

Pairwise distance metrics—Several pairwise distance metrics (ie, Euclidean, cosine, correlation, Minkowski) were tested on the PN data, and the one that best clustered both spiking and subthreshold responses from PNs of the same glomerular types was chosen for all subsequent analysis (correlation distance). Using cosine distances on the KCs (formula below) produced qualitatively similar results as when correlation distances were used. The distance between each pair of cells was inserted into the appropriate row and column of the distance

NIH-PA Author Manuscript

NIH-PA Author Manuscript

NIH-PA Author Manuscript

matrix (for example, see Figure 3C). Pairwise distances between either KC or PN responses (either subthreshold or PSTH) were calculated as follows: For each cell pair, we determined the number of tested odors in common. The 2s responses (odor stimulus + 1s; formed as described above) for only those odors were concatenated into a vector for each cell (r and s), and the distance between the two vectors was determined. Cosine distance was calculated as: $d(cos)=1-\alpha$, where $\alpha=rs'/(rr')^{1/2}(ss')^{1/2}$ (' denotes the transpose). Correlation distance was calculated as: $d(corr)=1-\beta$, where $\beta=(r\text{-}mean(r))(s\text{-}mean(s))'/[(r\text{-}mean(r))(r\text{-}mean(r))']^{1/2}[(s\text{-}mean(s))(s\text{-}mean(s)')]^{1/2}$. The correlation distance metric was also chosen to ensure that a uniform re-scaling of the gain of either response in a pair did not affect the distance between the pair.

Hierarchical clustering—For each resulting distance matrix, the rows (each row contains the pairwise distances between one cell and all other cells in the matrix) were compared using hierarchical clustering. We used the average linkage algorithm, which forms clusters between two groups (r and s) based on the average distance between all pairs of objects in cluster r and cluster s. If n_r is the number of cells in cluster r and n_s is the number of cells in cluster s, and x_{ri} is the *i*th object in cluster r and x_{sj} is the *j*th object in cluster s, the definition of the average linkage method is: $distance(r,s)=(1/n_r n_s)*(\sum i=1 \text{ to } n_r)(\sum j=1 \text{ to } n_s)dist(x_{ri},,x_{sj})$, where *dist*=Euclidean distance weight function.

Statistics—All p values reported in this study are two-tailed values and derived from a Student's t test, assuming unequal variances.

(1) Predicted number of non-singletons if replicates exist: We numerically computed the cumulative probability of finding ≥ N non-singletons (in any combination of groupings) for *n*=27 recordings from *m*=20 to 31 KC types (*n* samples drawn with replacement from a bag with *m* differently colored balls). The results are plotted in Figure 1E and 1F.

(2) K–L divergence: We quantified the similarity between a pair of distributions ($P_1(x)$, $P_2(x)$) with the standard Kullback-Leibler divergence: $D(P_1 \| P_2)=sum_x[P_1(x) \log_2(P_1(x)/P_2(x))]$. Reported K–L divergences (Figure 5D) represent averages over 100 trials, each trial comparing the distance distributions of 27 mKC types (gray curves, Figure 5C) or 27 individuals of one mKC type (light red curves, Figure 5C) to each other or to the distance distribution of the 27 recorded GFP^+ L-LP KCs (green curve, Figure 5C).

(3) Goodness-of-clustering scores: a)*Nearest neighbors method*: We assessed the goodness-of-clustering for PNs (Figure 4) and KC split trials (supplemental data) by whether closest linkages in the dendrogram were between PNs of the same glomerular types (*i.e.*, DL1, VC3, DM6) or between split trials. We divided the number of PNs that did not group by glomerular type or the number of KCs that did not group across their split trials by the total number of cells in the dendrogram, and then subtracted this value from 1 to arrive at an overall goodness-of-clustering score for the particular dendrogram. b)*Forced grouping method*: this score was calculated by forcing the pairwise distance data between mKCs into *N* groups, where *N* was pre-determined by the known number of mKC types in the data-set, and then subtracting from 1 the fraction of data that were assigned to the wrong group; group identity was defined by the mKC type most represented in that group. Over this procedure, no two groups shared the same identity. Goodness-of-clustering scores in Figure 5D were computed from 20 trials, each trial containing 23 mKC types and 10 individuals of each type.

KC simulations

Generation of mPNs—The data and results in Figure 5 and Figure 6 were generated using the temporal-shift procedure (method a below). The mPN responses generated with this method

NIH-PA Author Manuscript

NIH-PA Author Manuscript

NIH-PA Author Manuscript

produced inter-mPN and PN-mPN response profile distances that fell within the range of inter-PN distances in the recorded set (supplemental data).

a)*Temporal-shift method*: We selected 79/81 PN PSTH curves and delayed the response onset by a random amount chosen uniformly from the interval of 0 to 300ms, generating 79 new PN PSTH curves. This strategy was based on the observation that the primary difference between recordings from a larger set of PNs (Bhandawat et al., 2007) and those sampled here was a wider range of temporal delays of response onset relative to odor onset. The distribution of distances between mKC and KC response profiles (Figure 5) overlapped best for mKCs formed from mPNs generated with the temporal-shift method (as compared to methods b and c below), serving as a post-hoc validation of this method. b)*Principal component analysis (PCA) method*: We used the 81 recorded PN PSTH curves, performed PCA, and used the measured probability distributions of the top 20 PCA coefficients, treated as independent variables, to randomly sample a new set of coefficients. With the associated principal components and new coefficients, we constructed 79 additional curves (for a total of 160 curves) with features that resembled the original traces. c) Only the original set of recorded PN PSTH curves were used as the mPN responses.

Generation of inter-individual variability—We observed that individual response variability roughly correlates with the mean response. To port the variability curves recorded from PN types sampled more than once (e.g., DL1) to different PN types, we first "whitened" the content of the variability curves using a normalization procedure. The resulting inter-individual variability is a reasonable match to the data (supplemental data). Using recordings of all odors for all PNs sampled more than once (DL1, VC3, and DM6), we constructed a library of 168 PN variance curves by grouping all individual spiking responses ($r_{\beta i}(t)$) from the same PN/odor combination (β), and subtracting from each response the mean type response ($<r_{\beta t}(t)>)_i$ for that PN/odor combination. We then multiplied each variability curve originating from a type β response by a normalization factor $n_\beta(t)$. $n_\beta(t)$ varies inversely with the amplitude of the instantaneous mean type response: $n_\beta(t)=(a-(|<(r_\beta(t)>|/\max_t(|<r_\beta(t)>|))/a$, where $1<a<\infty$. This factor ranges from 1 for $|<(r_\beta(t)>|=0$ to (a-1)/a for $|<(r_\beta(t)>|=\max_t(|<r_\beta(t)>|$. When the parameter $a \rightarrow \infty$ the factor $(a-1)/a \rightarrow 1$, so there is almost no re-normalization. When $(a-1) \rightarrow 0$, rescaling is strong, because $(a-1)/a \rightarrow 0$. In our simulations, a=1.1. To generate individually varying mKC responses, we first chose a PN:KC weight vector (a binary vector of 0's and 1's, with a random set of N_{conv} entries set to 1) and generated an mKC type response (different mKC types were generated using different random PN:KC weight vectors). For each γth mPN type response $<r_\gamma(t)>$ with a non-zero entry in the weight vector, we then randomly selected a variability curve from the full library, and multiplied it with the inverse normalization factor $n_\gamma(t)^{-1}=a*(a-(|<(r_\gamma(t)>|/\max_t(|<r_\gamma(t)>|))^{-1}$ to produce a scaled variability trace that roughly co-varied with the selected mPN type; we added this variability to $<r_\gamma(t)>$ to produce an individual version of that type response, and repeated this for all mPNs selected by the weight vector. These summed curves produced one individual mKC response for that type. Reconstructing the model using only un-normalized individual variability curves produced better separation between inter-individual and inter-type distances, leading to better clustering (data not shown). Thus, the normalization procedure produced more conservative statements about KC identifiability.

Sampling experiment—For each run of the sampling experiment, we randomly selected 27 individual curves from a newly generated set of mKCs consisting of 27 individuals each of 23 types. The experiment was repeated 2000 times (for each N_{conv}).

Varying PN:KC weights and connectivity—To determine the effect of varying PN:KC weights on KC response variability, we assigned each mKC type a binary PN:KC weight vector, as before, but allowed the weights for the nonzero entries of the binary connection

NIH-PA Author Manuscript

NIH-PA Author Manuscript

NIH-PA Author Manuscript

matrix to take analog values. For each individual of a type, the non-zero weights were selected randomly from the interval [1−p,1+p], where p refers to the percent variability allowed in the weights, and ranged from 0 to 0.8. To determine the effect of varying PN:KC connectivity on KC response variability, we defined each mKC type by an archetypal binary PN:KC weight vector. Individual mKCs were generated from the archetype weight vector by selecting a fraction p of the non-zero entries, setting them to zero, and randomly selecting an equal number of new non-zero entries. As above, p refers to the percent variability, and ranged from 0 to 0.8. Figure 6D was generated from these model KC data using the methods described under Sampling experiment.

Supplementary Material

Refer to Web version on PubMed Central for supplementary material.

ACKNOWLEDGEMENTS

We are grateful to Kai Zinn for the use of his laboratory to rear flies and establish crosses, to Glenn Turner for help in establishing recording techniques from Kenyon cells, to Kei Ito for the gifts of *NP7175-GAL4* and *NP3529-GAL4*, to Philip Coen for help with the anatomical identification of KCs, to the Caltech Biological Imaging Center for use of confocal microscopes, to members of the Laurent lab for advice, and to David Anderson, Benjamin Rubin, Kai Zinn, Glenn Turner, and Timothy Tayler for providing comments on this manuscript. MM is a Helen Hay Whitney Foundation Postdoctoral Fellow and IF is a Senior Broad Fellow in Brain Circuitry. This work was funded by grants from the NIDCD, the NSF BITS Program and the Lawrence Hanson Fund (GL).

REFERENCES

Belluscio L, Katz LC. Symmetry, stereotypy, and topography of odorant representations in mouse olfactory bulbs. J Neurosci 2001;21:2113–2122. [PubMed: 11245695]

Berdnik D, Chihara T, Couto A, Luo L. Wiring stability of the adult Drosophila olfactory circuit after lesion. J Neurosci 2006;26:3367–3376. [PubMed: 16571743]

Bhandawat V, Olsen SR, Gouwens NW, Schlief ML, Wilson RI. Sensory processing in the Drosophila antennal lobe increases reliability and separability of ensemble odor representations. Nature neuroscience. 2007

Brand AH, Perrimon N. Targeted gene expression as a means of altering cell fates and generating dominant phenotypes. Development (Cambridge, England) 1993;118:401–415.

Couto A, Alenius M, Dickson BJ. Molecular, anatomical, and functional organization of the Drosophila olfactory system. Curr Biol 2005;15:1535–1547. [PubMed: 16139208]

Crittenden JR, Skoulakis EM, Han KA, Kalderon D, Davis RL. Tripartite mushroom body architecture revealed by antigenic markers. Learning & memory (Cold Spring Harbor, N.Y 1998;5:38–51.

Daniels RW, Gelfand MV, Collins CA, DiAntonio A. Visualizing glutamatergic cell bodies and synapses in Drosophila larval and adult CNS. The Journal of comparative neurology 2008;508:131–152. [PubMed: 18302156]

Davis RL. Mushroom bodies and Drosophila learning. Neuron 1993;11:1–14. [PubMed: 8338661]

Davis RL. Olfactory memory formation in Drosophila: from molecular to systems neuroscience. Annual review of neuroscience 2005;28:275–302.

de Bruyne M, Foster K, Carlson JR. Odor coding in the Drosophila antenna. Neuron 2001;30:537–552. [PubMed: 11395013]

Dobritsa AA, van der Goes van Naters W, Warr CG, Steinbrecht RA, Carlson JR. Integrating the molecular and cellular basis of odor coding in the Drosophila antenna. Neuron 2003;37:827–841. [PubMed: 12628173]

Dubnau J, Grady L, Kitamoto T, Tully T. Disruption of neurotransmission in Drosophila mushroom body blocks retrieval but not acquisition of memory. Nature 2001;411:476–480. [PubMed: 11373680]

Fishilevich E, Vosshall LB. Genetic and functional subdivision of the Drosophila antennal lobe. Curr Biol 2005;15:1548–1553. [PubMed: 16139209]

NIH-PA Author Manuscript

NIH-PA Author Manuscript

NIH-PA Author Manuscript

Gerber B, Tanimoto H, Heisenberg M. An engram found? Evaluating the evidence from fruit flies. Current opinion in neurobiology 2004;14:737–744. [PubMed: 15582377]

Gu H, O'Dowd DK. Cholinergic synaptic transmission in adult Drosophila Kenyon cells in situ. J Neurosci 2006;26:265–272. [PubMed: 16399696]

Halfon MS, Gisselbrecht S, Lu J, Estrada B, Keshishian H, Michelson AM. New fluorescent protein reporters for use with the Drosophila Gal4 expression system and for vital detection of balancer chromosomes. Genesis 2002;34:135–138. [PubMed: 12324968]

Hallem EA, Carlson JR. The odor coding system of Drosophila. Trends Genet 2004;20:453–459. [PubMed: 15313555]

Hallem EA, Ho MG, Carlson JR. The molecular basis of odor coding in the Drosophila antenna. Cell 2004;117:965–979. [PubMed: 15210116]

Han PL, Levin LR, Reed RR, Davis RL. Preferential expression of the Drosophila rutabaga gene in mushroom bodies, neural centers for learning in insects. Neuron 1992;9:619–627. [PubMed: 1382471]

Heisenberg M, Borst A, Wagner S, Byers D. Drosophila mushroom body mutants are deficient in olfactory learning. Journal of neurogenetics 1985;2:1–30. [PubMed: 4020527]

Heisenberg M, Heusipp M, Wanke C. Structural plasticity in the Drosophila brain. J Neurosci 1995;15:1951–1960. [PubMed: 7891144]

Ito K, Awano W, Suzuki K, Hiromi Y, Yamamoto D. The Drosophila mushroom body is a quadruple structure of clonal units each of which contains a virtually identical set of neurones and glial cells. Development (Cambridge, England) 1997;124:761–771.

Jefferis GS, Marin EC, Stocker RF, Luo L. Target neuron prespecification in the olfactory map of Drosophila. Nature 2001;414:204–208. [PubMed: 11719930]

Jefferis GS, Potter CJ, Chan AM, Marin EC, Rohlfing T, Maurer CR Jr, Luo L. Comprehensive maps of Drosophila higher olfactory centers: spatially segregated fruit and pheromone representation. Cell 2007;128:1187–1203. [PubMed: 17382886]

Jefferis GS, Vyas RM, Berdnik D, Ramaekers A, Stocker RF, Tanaka NK, Ito K, Luo L. Developmental origin of wiring specificity in the olfactory system of Drosophila. Development (Cambridge, England) 2004;131:117–130.

Komiyama T, Luo L. Development of wiring specificity in the olfactory system. Current opinion in neurobiology 2006;16:67–73. [PubMed: 16377177]

Krashes MJ, Keene AC, Leung B, Armstrong JD, Waddell S. Sequential use of mushroom body neuron subsets during drosophila odor memory processing. Neuron 2007;53:103–115. [PubMed: 17196534]

Kurusu M, Awasaki T, Masuda-Nakagawa LM, Kawauchi H, Ito K, Furukubo-Tokunaga K. Embryonic and larval development of the Drosophila mushroom bodies: concentric layer subdivisions and the role of fasciclin II. Development (Cambridge, England) 2002;129:409–419.

Laissue PP, Reiter C, Hiesinger PR, Halter S, Fischbach KF, Stocker RF. Three-dimensional reconstruction of the antennal lobe in Drosophila melanogaster. The Journal of comparative neurology 1999;405:543–552. [PubMed: 10098944]

Lee T, Lee A, Luo L. Development of the Drosophila mushroom bodies: sequential generation of three distinct types of neurons from a neuroblast. Development (Cambridge, England) 1999;126:4065–4076.

Lewis EB. Drosophila Information Service. 1960;34

Lin HH, Lai JS, Chin AL, Chen YC, Chiang AS. A map of olfactory representation in the Drosophila mushroom body. Cell 2007;128:1205–1217. [PubMed: 17382887]

Margulies C, Tully T, Dubnau J. Deconstructing memory in Drosophila. Curr Biol 2005;15:R700–R713. [PubMed: 16139203]

Marin EC, Jefferis GS, Komiyama T, Zhu H, Luo L. Representation of the glomerular olfactory map in the Drosophila brain. Cell 2002;109:243–255. [PubMed: 12007410]

Marin EC, Watts RJ, Tanaka NK, Ito K, Luo L. Developmentally programmed remodeling of the Drosophila olfactory circuit. Development (Cambridge, England) 2005;132:725–737.

NIH-PA Author Manuscript

NIH-PA Author Manuscript

NIH-PA Author Manuscript

Masuda-Nakagawa LM, Tanaka NK, O'Kane CJ. Stereotypic and random patterns of connectivity in the larval mushroom body calyx of Drosophila. Proceedings of the National Academy of Sciences of the United States of America 2005;102:19027–19032. [PubMed: 16357192]

McGuire SE, Le PT, Davis RL. The role of Drosophila mushroom body signaling in olfactory memory. Science (New York, N.Y 2001;293:1330–1333.

McGuire SE, Le PT, Osborn AJ, Matsumoto K, Davis RL. Spatiotemporal rescue of memory dysfunction in Drosophila. Science (New York, N.Y 2003;302:1765–1768.

Meister M, Bonhoeffer T. Tuning and topography in an odor map on the rat olfactory bulb. J Neurosci 2001;21:1351–1360. [PubMed: 11160406]

Menzel R. Neurobiology of learning and memory: the honeybee as a model system. Die Naturwissenschaften 1983;70:504–511. [PubMed: 6656885]

Mombaerts P, Wang F, Dulac C, Chao SK, Nemes A, Mendelsohn M, Edmondson J, Axel R. Visualizing an olfactory sensory map. Cell 1996;87:675–686. [PubMed: 8929536]

Ng M, Roorda RD, Lima SQ, Zemelman BV, Morcillo P, Miesenbock G. Transmission of olfactory information between three populations of neurons in the antennal lobe of the fly. Neuron 2002;36:463–474. [PubMed: 12408848]

Nighorn A, Healy MJ, Davis RL. The cyclic AMP phosphodiesterase encoded by the Drosophila dunce gene is concentrated in the mushroom body neuropil. Neuron 1991;6:455–467. [PubMed: 1848082]

Olsen SR, Bhandawat V, Wilson RI. Excitatory interactions between olfactory processing channels in the Drosophila antennal lobe. Neuron 2007;54:89–103. [PubMed: 17408580]

Perez-Orive J, Mazor O, Turner GC, Cassenaer S, Wilson RI, Laurent G. Oscillations and sparsening of odor representations in the mushroom body. Science (New York, N.Y 2002;297:359–365.

Quinn WG, Harris WA, Benzer S. Conditioned behavior in Drosophila melanogaster. Proceedings of the National Academy of Sciences of the United States of America 1974;71:708–712. [PubMed: 4207071]

Ressler KJ, Sullivan SL, Buck LB. Information coding in the olfactory system: evidence for a stereotyped and highly organized epitope map in the olfactory bulb. Cell 1994;79:1245–1255. [PubMed: 7528109]

Rubin BD, Katz LC. Optical imaging of odorant representations in the mammalian olfactory bulb. Neuron 1999;23:499–511. [PubMed: 10433262]

Schwaerzel M, Heisenberg M, Zars T. Extinction antagonizes olfactory memory at the subcellular level. Neuron 2002;35:951–960. [PubMed: 12372288]

Schwartz YB, Boykova T, Belyaeva ES, Ashburner M, Zhimulev IF. Molecular characterization of the singed wings locus of Drosophila melanogaster. BMC genetics 2004;5:15. [PubMed: 15189568]

Shang Y, Claridge-Chang A, Sjulson L, Pypaert M, Miesenbock G. Excitatory local circuits and their implications for olfactory processing in the fly antennal lobe. Cell 2007;128:601–612. [PubMed: 17289577]

Stopfer M, Jayaraman V, Laurent G. Intensity versus identity coding in an olfactory system. Neuron 2003;39:991–1004. [PubMed: 12971898]

Stopfer M, Laurent G. Short-term memory in olfactory network dynamics. Nature 1999;402:664–668. [PubMed: 10604472]

Strausfeld NJ, Sinakevitch I, Vilinsky I. The mushroom bodies of Drosophila melanogaster: an immunocytological and golgi study of Kenyon cell organization in the calyces and lobes. Microscopy research and technique 2003;62:151–169. [PubMed: 12966500]

Tamura T, Chiang AS, Ito N, Liu HP, Horiuchi J, Tully T, Saitoe M. Aging specifically impairs amnesiac-dependent memory in Drosophila. Neuron 2003;40:1003–1011. [PubMed: 14659098]

Tanaka NK, Awasaki T, Shimada T, Ito K. Integration of chemosensory pathways in the Drosophila second-order olfactory centers. Curr Biol 2004;14:449–457. [PubMed: 15043809]

Technau GM. Fiber number in the mushroom bodies of adult Drosophila melanogaster depends on age, sex and experience. Journal of neurogenetics 1984;1:113–126. [PubMed: 6085635]

Turner GC, Bazhenov M, Laurent G. Olfactory Representations by Drosophila Mushroom Body Neurons. Journal of neurophysiology. 2007

NIH-PA Author Manuscript

NIH-PA Author Manuscript

NIH-PA Author Manuscript

Uchida N, Takahashi YK, Tanifuji M, Mori K. Odor maps in the mammalian olfactory bulb: domain organization and odorant structural features. Nature neuroscience 2000;3:1035–1043.

Vassar R, Chao SK, Sitcheran R, Nunez JM, Vosshall LB, Axel R. Topographic organization of sensory projections to the olfactory bulb. Cell 1994;79:981–991. [PubMed: 8001145]

Vosshall LB, Stocker RF. Molecular Architecture of Smell and Taste in Drosophila. Annual review of neuroscience. 2006

Wang JW, Wong AM, Flores J, Vosshall LB, Axel R. Two-photon calcium imaging reveals an odor-evoked map of activity in the fly brain. Cell 2003;112:271–282. [PubMed: 12553914]

Wang Y, Guo HF, Pologruto TA, Hannan F, Hakker I, Svoboda K, Zhong Y. Stereotyped odor-evoked activity in the mushroom body of Drosophila revealed by green fluorescent protein-based Ca2+ imaging. J Neurosci 2004;24:6507–6514. [PubMed: 15269261]

Wilson RI, Turner GC, Laurent G. Transformation of olfactory representations in the Drosophila antennal lobe. Science (New York, N.Y 2004;303:366–370.

Wong AM, Wang JW, Axel R. Spatial representation of the glomerular map in the Drosophila protocerebrum. Cell 2002;109:229–241. [PubMed: 12007409]

Yasuyama K, Meinertzhagen IA, Schurmann FW. Synaptic organization of the mushroom body calyx in Drosophila melanogaster. The Journal of comparative neurology 2002;445:211–226. [PubMed: 11920702]

Zars T, Fischer M, Schulz R, Heisenberg M. Localization of a short-term memory in Drosophila. Science (New York, N.Y 2000;288:672–675.

Zhu S, Chiang AS, Lee T. Development of the Drosophila mushroom bodies: elaboration, remodeling and spatial organization of dendrites in the calyx. Development (Cambridge, England) 2003;130:2603–2610.

NIH-PA Author Manuscript
NIH-PA Author Manuscript
NIH-PA Author Manuscript

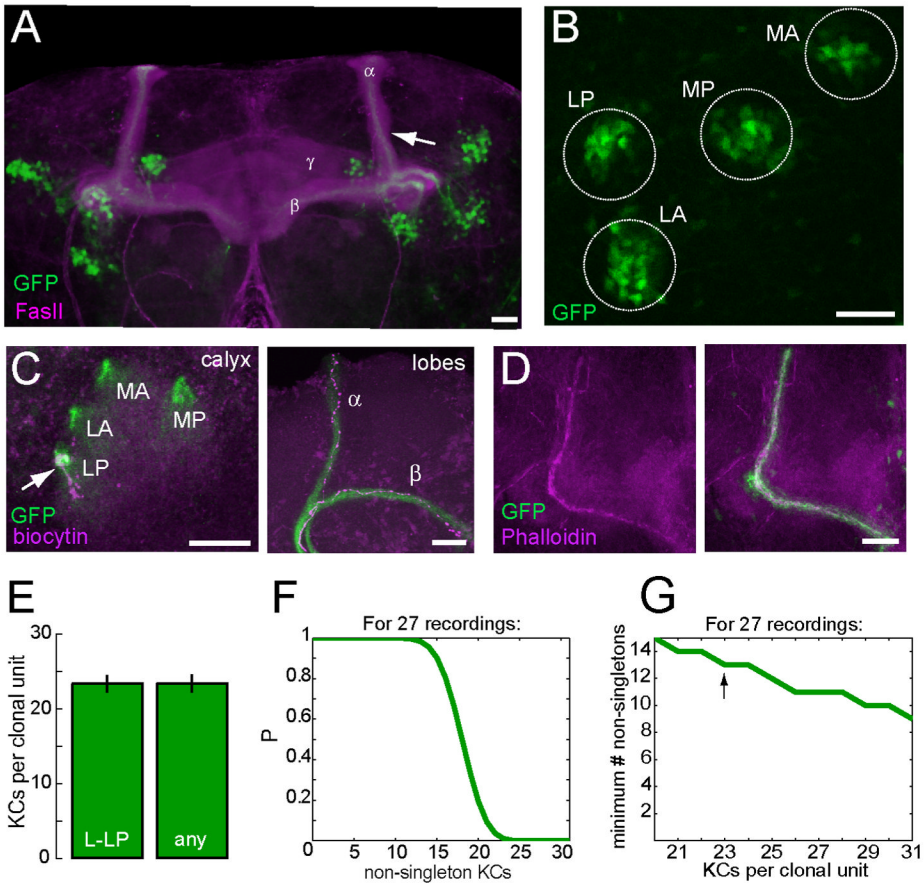

Figure 1. NP7175-GAL4 labels a small subset of α/β KCs, and facilitates recordings from potential KC replicates across flies

A. KCs labeled in *NP7175-GAL4; UAS-eGFP2x/Cyo* flies (green) project to the centers of the α/β lobes (arrow). Anti-FasII (magenta) labels both the α/β and γ lobes of the MB.

B. NP7175 labels KCs that can be subdivided into 4 clonal units. Each clonal unit innervates one of the four sectors of the MB calyx: lateral anterior (LA), lateral posterior (LP), medial anterior (MA), or medial posterior (MP).

C. (left) Each KC in the data set (shown here, KC2) was filled with biocytin (magenta) during the recording in order to identify, post-hoc, if it was or was not GFP^+, and if GFP^+, to confirm that its dendrites (arrow) innervated the LP region of the calyx. (right) Fill of KC11 imaged in the lobes.

D. GFP expression in KC axons co-localized with Phalloidin in the centers of the α/β lobes (magenta; labels F-actin-enriched fibers).

E. Counts of the number of cells labeled by NP7175 per clonal unit from only the LP clonal unit, left hemisphere (8 brains) or any clonal unit, either hemisphere (4 brains and 12 clonal units). Error bars are SEM.

F. For 27 KC recordings from the 23-cell GFP^+ L-LP clonal unit, the cumulative probability (P) of recording from non-singleton (replicate) KCs, assuming they exist.

G. For 27 KC recordings, the minimum number (with P>0.99) of non-singletons in the data set as a function of the total number of GFP^+ cells per clonal unit. The arrow indicates the minimum number of non-singletons corresponding to 23 GFP^+ KCs per clonal unit.

All images are projections of confocal stacks. Dorsal is up, and all scale bars = 20μm.

NIH-PA Author Manuscript
NIH-PA Author Manuscript
NIH-PA Author Manuscript

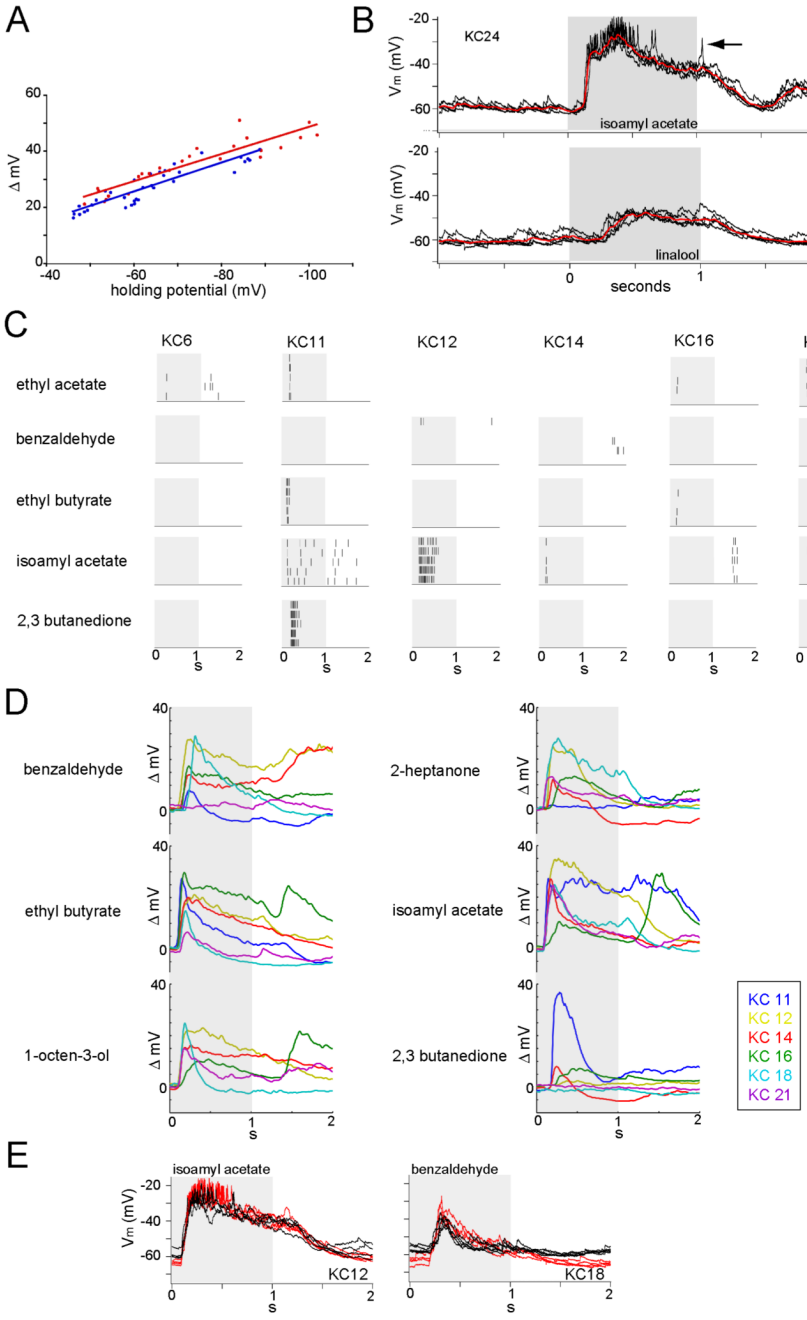

Figure 2. Kenyon cell odor responses

A. Relationship between holding potential and the amount of depolarization (ΔmV) evoked by an odor for two different KCs (red and blue), both tested with isoamyl acetate [1/100]. Holding potential was measured as the average V_m during the 100ms before odor onset, and ΔmV was calculated as V_{max} during the odor response (odor onset + 3s) of each smoothed trace minus the holding potential. R^2 of the linear fit for the blue cell = 0.827; for the red cell = 0.8435.

B. Example raw data from one KC. Voltage traces for 5 trials (trials 2–6 (1st trial excluded for all analyses)) of odor responses to isoamyl acetate [1/100] (produced spikes, arrow) and linalool

NIH-PA Author Manuscript

NIH-PA Author Manuscript

NIH-PA Author Manuscript

[1/100] (did not produce spikes). The odor stimulus (light gray bar) occurs at time 0 and lasts for 1s. Subthreshold odor responses (trial-averaged) are overlaid in red.

C. Spike rasters for 5 odors and 6 GFP^+ L-LP KCs; ethyl acetate was not tested on KCs 12 and 14. All odors shown were delivered at [1/100]. Each KC in the data set was tested with 10 different odors, on average.

D. Subthreshold odor responses for 6 odors (all presented at [1/100]) and 6 GFP^+ L-LP KCs.

E. Stability of KC responses during a recording: raw membrane voltage traces from KC12 (left) and KC18 (right) for the same odor presented at the beginning (red trials) and end (black trials) of each experiment.

NIH-PA Author Manuscript
NIH-PA Author Manuscript
NIH-PA Author Manuscript

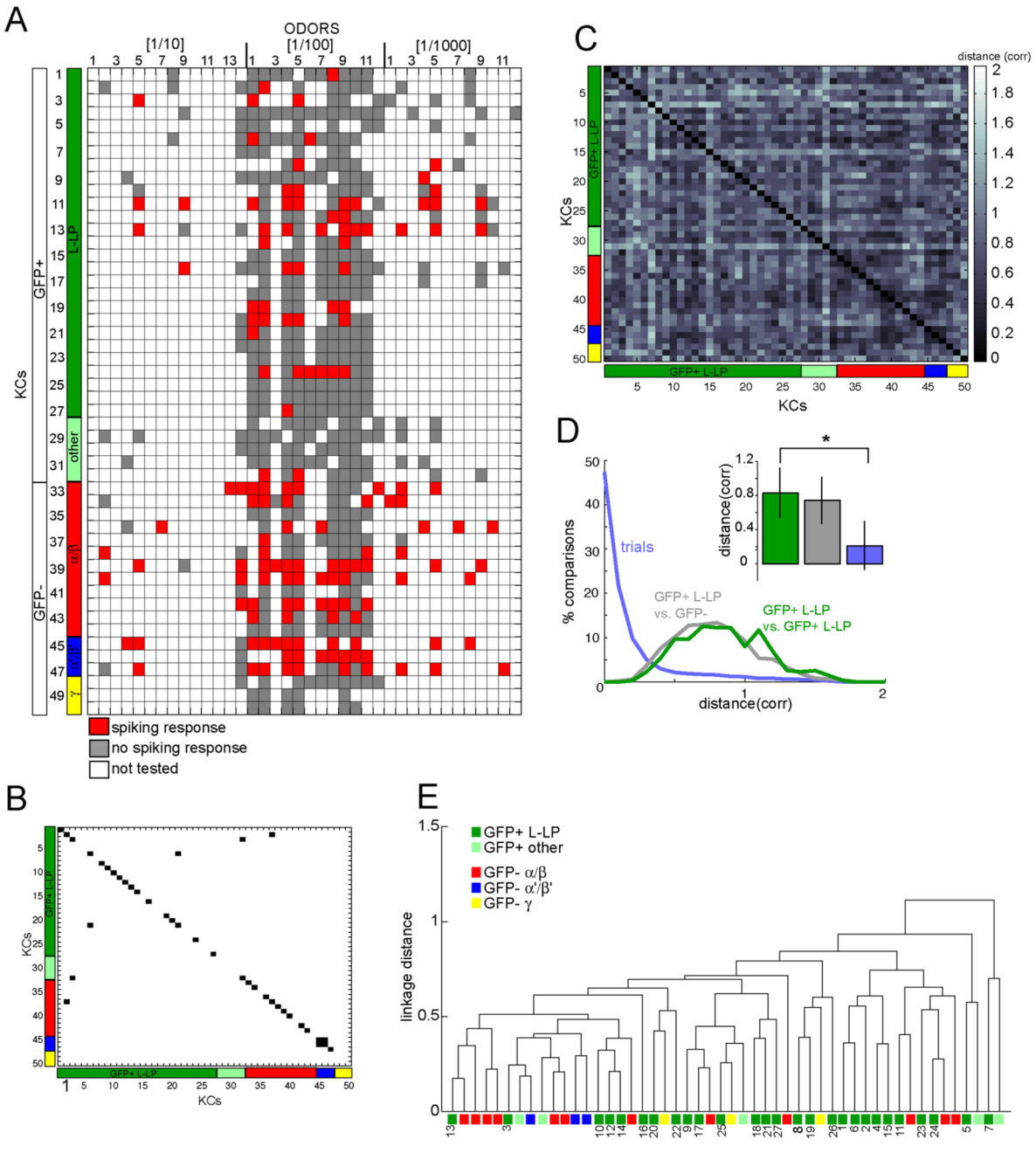

Figure 3. Lack of obvious functional replicates among the GFP$^+$ L-LP KC recordings

A. Odor response chart: odors were chosen from a set of 38 (12 odors delivered at 3 different final concentrations, [1/10], [1/100], and [1/1000], and 2 odors delivered only at [1/10] (see methods for odor identities)). For each odor tested, response (red) = spikes on 3 or more trials, and no response (gray) = spikes on 2 or fewer trials. White boxes indicate odors not tested. Cells 1–27 are from the GFP$^+$ L-LP clonal unit, 28–32 are GFP$^+$ from other clonal units, 33–44 are GFP$^-$ α/β, 45–47 are GFP$^-$ α'/β', and 48–50 are GFP$^-$ γ. The somata of recorded GFP$^-$ cells were located adjacent to GFP$^+$ somata, mostly from the L-LP clonal unit.

B. Pairwise Euclidean distances between odor response profiles (rows in A). A distance of 0 (black) indicates that odor response profiles are identical and non-zero for the KC pair.

NIH-PA Author Manuscript

NIH-PA Author Manuscript

NIH-PA Author Manuscript

Distances >0 and KC pairs with no responses to any common odors (spikes on 2 or fewer trials) are colored white.

C. Pairwise correlation distances based on subthreshold odor responses (correlation distances can range from 0 (perfect correlation) to 2 (anti-correlation)) for all 50 KCs, and for all odors tested in common between each pair of cells.

D. Probability distributions (smoothed histograms; bin size = 0.1) of pairwise correlation distances in C. The distribution of distances between only GFP^+ L-LP cells (green) overlaps the distribution of distances between GFP^+ L-LP cells and GFP^- cells (gray), as do the means and standard deviations of the distributions (inset). The distribution of distances between trials for each KC/odor combination (blue) is significantly smaller than the inter-KC distances. * for Student's t test between GFP^+ L-LP distances and trial-trial distances, $p<10^{-87}$.

E. Hierarchical clustering of all KCs (based on average linkage of pairwise distances shown in C). The identities (1–27) of GFP^+ L-LP KCs (dark green) are indicated below the corresponding leaves of the tree.

NIH-PA Author Manuscript
NIH-PA Author Manuscript
NIH-PA Author Manuscript

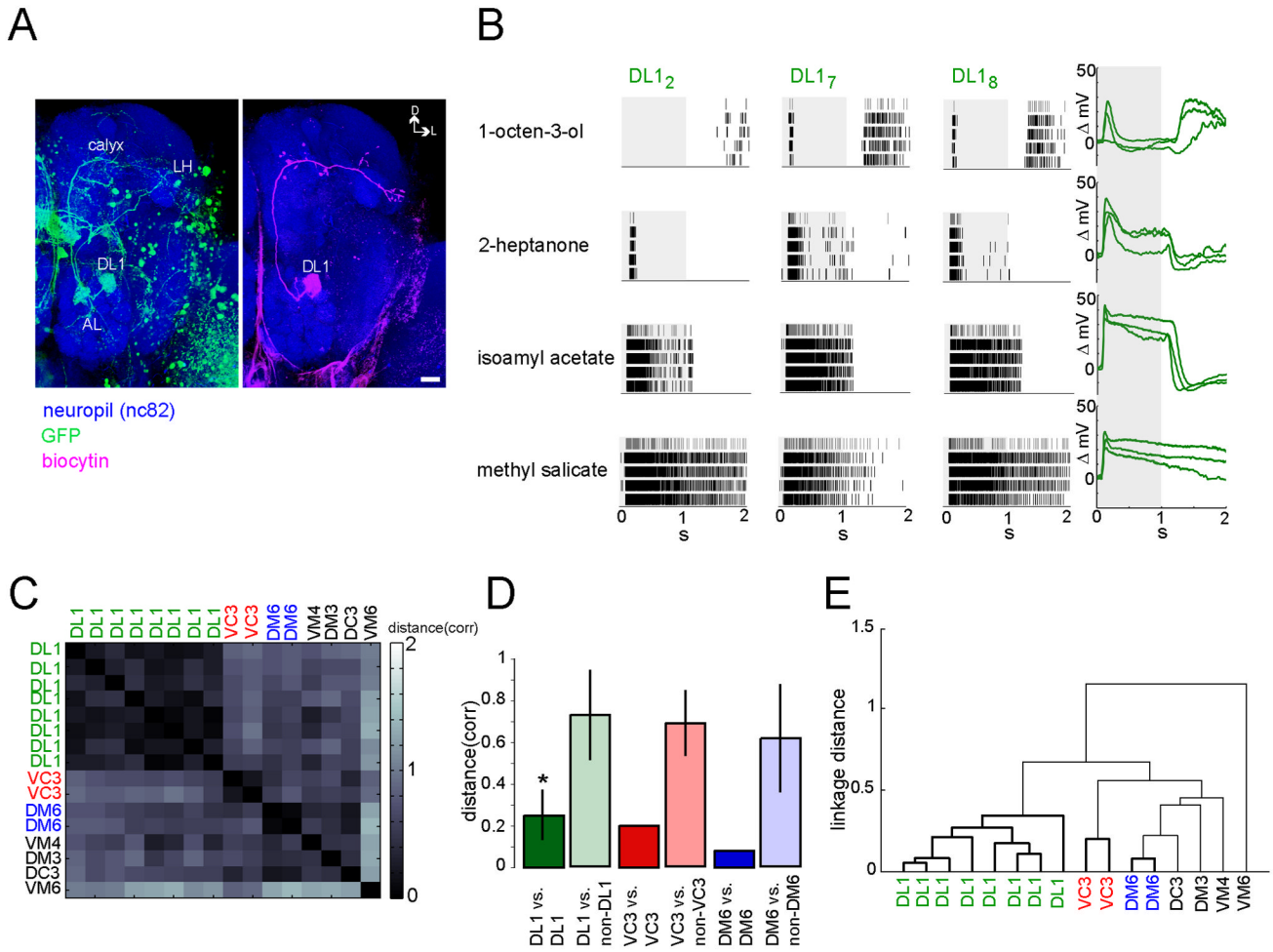

Figure 4. Quantification of odor response variability across PNs of the same glomerular type

A. Confocal projection of the fill of one recorded DL1 PN from a fly of genotype *UAS-eGFP2x; NP3529-GAL4*. AL = antennal lobe; LH = lateral horn. Scale bar = 20 μm, and dorsal is up.

B. Spike rasters and subthreshold odor responses (trial-averaged) for 4 odors (delivered at [1/100]) and 3 DL1 PNs. Odor onset occurs at time 0 and lasts for 1s. Each PN in the data set was tested with 11 odors, on average.

C. Pairwise correlation distances between subthreshold odor responses for 16 PNs and all odors tested in common between each pair.

D. Mean ± SD for pairwise subthreshold correlation distances: DLI-DL1 distances (green), DL1-nonDL1 distances (light green), VC3-VC3 distance (red), VC3-nonVC3 distances (light red), DM6-DM6 distance (blue), and DM6-nonDM6 distances (light blue). * for Student's t test between DL1-DL1 distances and DL1-nonDL1 distances, $p<10^{-23}$.

E. Hierarchical clustering of all PNs (based on average linkage of pairwise distances shown in C).

NIH-PA Author Manuscript

NIH-PA Author Manuscript

NIH-PA Author Manuscript

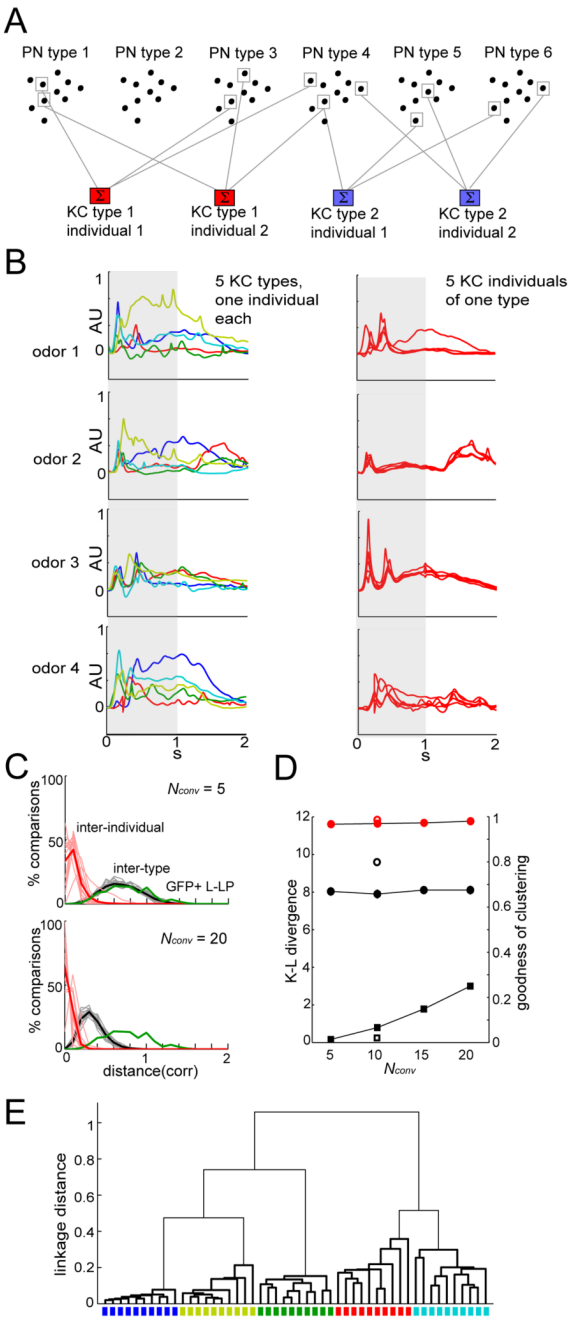

Figure 5. Model KCs formed by linear summation of PN responses can be clustered by type despite individual variability

A. Cartoon of the model: simulated KCs (colored boxes) were generated by summation of multiple PN odor response profiles (black circles). Each PN response profile represents responses across 4 virtual odors. We diagram here the production of 2 KC types and 2 replicates (individuals) of each type, using a convergence of 3,.

B. Examples of model KC (mKC) responses, formed with PN:KC convergence (N_{conv})=5*2 (convergence of 10 PNs of 5 different types onto 1 KC). Shown here are responses across 4 virtual odors for 5 mKCs of different types (left) and 5 mKCs of one type (right). AU = arbitrary units.

NIH-PA Author Manuscript

NIH-PA Author Manuscript

NIH-PA Author Manuscript

C. Probability distributions of mKC (red and black curves) and GFP^+ L-LP KC (green curves; reproduced from Figure 3D) pairwise distances for N_{conv}=5 and 20; bin size=0.1. To compare with the real data, we plot the distributions of correlation distances between 27 mKCs of different types (15 examples, gray) or between 27 individuals of a single mKC type (15 examples, light red). The average over 100 such curves is overlaid in black (inter-type distances) or red (inter-individual distances).

D. Kulblack-Leibler (K–L) divergences between mKC inter-type distances and GFP^+ L-LP distances grew with increasing N_{conv} (black squares). However, K–L divergences between mKC inter-type and inter-individual distances were not affected by N_{conv} (black circles). The goodness-of-clustering score (red circles) is a measure of how well mKCs group by type through hierarchical clustering (see E). Scores for N_{conv}=5*2 are plotted as open circles and squares. A K–L divergence of 0 indicates a perfect overlap between two distributions. Error bars are SEM.

E. The data in B for 5 mKC types (shown here 10 individuals of each type) was easily clustered by type. Colored squares correspond to the different KC types shown in B.

NIH-PA Author Manuscript
NIH-PA Author Manuscript
NIH-PA Author Manuscript

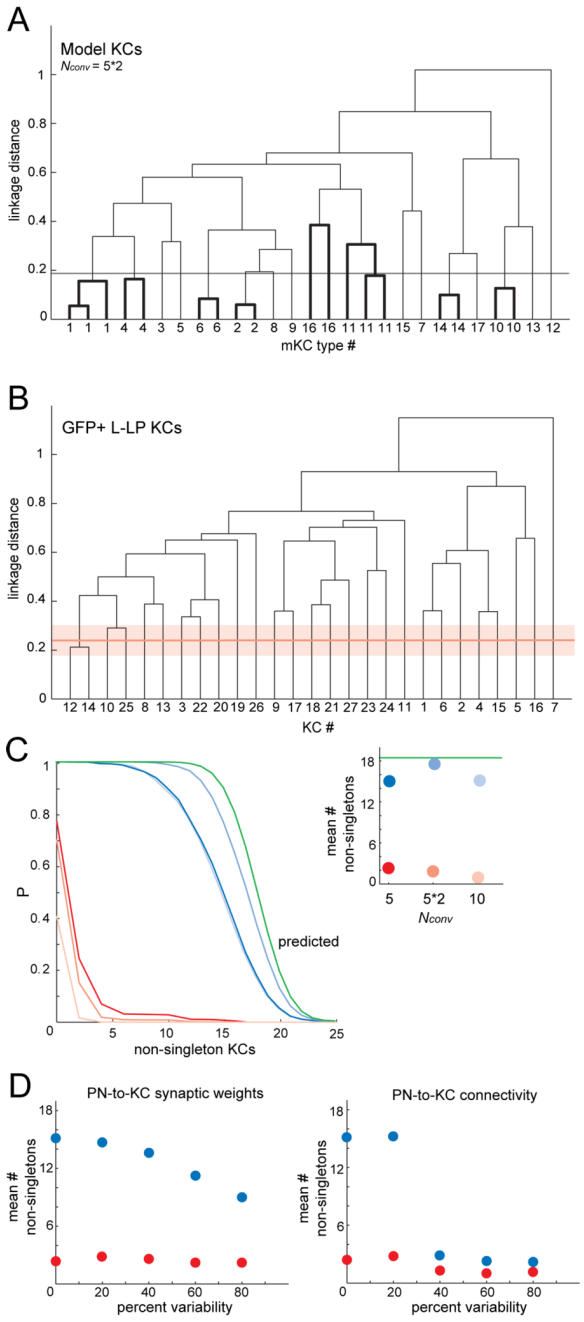

Figure 6. Clustering thresholds from the model applied to the data indicate few potential replicates

A. One run of the sampling experiment for N_{conv}=5*2. The numbers on the abscissa indicate different mKC types. The gray line is, for this dendrogram, the highest threshold below which all groupings are only between non-singleton mKCs (correct groupings – thick black lines). Above the threshold there is at least one grouping between mKCs of different types (e.g., mKCs of type 2 with an mKC of type 8).

B. Hierarchical clustering of only GFP$^+$ L-LP KCs. The red line is drawn at the mean value from 2000 thresholds for N_{conv}=5*2, each threshold derived from a run of the sampling experiment (as in A). The light red box indicates the 10–90% range of these thresholds.

NIH-PA Author Manuscript

NIH-PA Author Manuscript

NIH-PA Author Manuscript

C. Cumulative probability distributions of identifying *n* non-singletons in the model (blue curves) or in the real data (red curves). From the sampling experiment, probability distributions were formed by thresholding the model dendrograms for each value of N_{conv}=5,5*2, or 10 (dark to light blue, respectively). Because thresholds miss linkages between individuals of one type with large variance, this method undercounts the true number of non-singletons in the dendrograms and the model (blue) probability distributions lie to the left of the predicted distribution (green; reproduced from Figure 1F). For the real data, probability distributions of finding *n* non-singletons are formed by applying, one at a time, the complete set of thresholds from the sampling experiment (for N_{conv}=5,5*2, or 10 (dark to light red curves, respectively)) to the dendrogram in B and counting the number of KCs with linkage distances below each threshold. Inset: average number of non-singletons predicted (green line) or identified using the thresholds in the model (blue) or in the real data (red).

D. For N_{conv}=5 only, the average number of KC non-singletons found (by the methods described above) in the model (blue) or in the real data (red) as the percent variability in either the synaptic weights (left) or identities of presynaptic PNs (right) was increased systematically from 0 to 80% across individuals.